MATEC Web of Conferences **21**, 06005 (2015)
DOI: 10.1051/matecconf/20152106005

Deformation behaviour of laser-welded tube blank of TA15 Ti-alloy for gas forming at elevated temperature

Kehuan Wang[1], Gang Liu[1,2,a], and Shijian Yuan[1,2]

[1] School of Materials Science and Engineering, Harbin Institute of Technology, Harbin150001, China
[2] National Key Laboratory for Precision Hot Processing of Metals, Harbin Institute of Technology, Harbin 150001, China

Abstract. Deformation behaviour of laser-welded tube blank of TA15 Ti-alloy at elevated temperature was investigated by both hot tensile tests and high pressure gas forming(HPGF). The hot tensile tests were carried out with four different specimens at 800 °C with an initial strain rate of 1.00×10^{-2} s^{-1} and HPGF test was performed at 800 °C with a constant pressure of 9.5MPa. The tensile results show that base material with equiaxed microstructure exhibited good formability and grain boundary sliding (GBS) accompanied with dynamic recrystallization (DRV) was the main deformation mechanism. However, because the weld bead has coarse columnar grains with fine acicular α' in the β matrix, when the loading direction is parallel with the weld bead, the fine acicular α' transformed into thicker α lamella and the aspect ratio decreased greatly, and voids formed along the initial coarse β grain boundaries. When the loading direction is vertical with the weld bead, the welded materials deformed little and the lamella structure thickened obviously after deformation. HPGF tests demonstrate that the laser-welded TA15 tube had a very good formability at 800 °C, and the maximum bulging ratio was as high as 77.4%.

1. Introduction

Ti-alloys are wildly used in aerospace industry due to their outstanding properties including superior strength-to-weight ratio and good elevated temperature performance [1]. Recently, in order to improve the performance of aircrafts, integrated and large size structures are needed [2]. However, because of the size limit of the rolled Ti alloy sheets, tailor welded blank becomes a good option [3]. A laser beam is a very concentrated energy source which could provide a high power density [4]. It has been demonstrated by lots of studies that laser beam welding (LBW) has considerable flexibility for joining titanium alloys [5], so LBW is widely applied in Ti-alloy tailor welded blank production [6]. Superplastic forming (SPF) is an efficient method to fabricate the complex Ti-alloy components [7]. The combination of SPF and LBW has been used to form Ti-alloy multi-sheet structures [8]. It was found that laser-welded Ti–6Al–4V alloy joint has a good formability under optimal SPF condition and a maximum elongation of 387% was achieved [9, 10]. Gang Wang etc. [10] also studied the superplasticity of TC4

[a] Corresponding author: gliu@hit.edu.cn

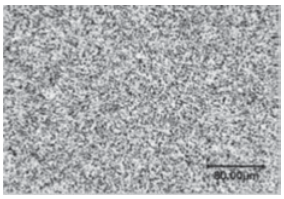

Figure 1. Microstructure of the as-received material.

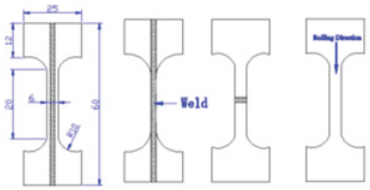

Figure 2. Sketch of the tensile specimens.

laser-welded joint by superplastic bulging tests. The welded Ti-alloy joints have lamellar microstructure in the weld zone, and continuous globularization ensures a good superplasticity of the material, so full globularization happened after superplastic deformation. However, to reduce cycle time and increase productivity, forming process at higher strain rate and lower temperature should be developed. G. Liu etc. [11] formed Ti-3Al-2.5V parts with seamless tube at temperature around 8000C by high pressure gas forming process (HPGF) successfully. Few reports were found about the deformation behaviour of laser-welded Ti-alloy tube blank within this kind of forming process, especially for Ti–6.5Al–2Zr–1Mo-1V (TA15) alloy.

2. Material and Experimental Procedures

A TA15 hot rolled sheet with a thickness of 2 mm was used in this study. Figure 1 shows the microstructure of the initial material. One can see that the material contains mostly equiaxed α grains with an average grain size of 3.2 μm and a small fraction of β phase (4–7%) dispersed between the α grains and at grain boundary triple points. The LBW was performed with a diffusion cooling carbon dioxide laser of 3.0 kW rated power (ROFIN-SINARDC030). The output power and the welding speed were 1.0kW and 1.2 m/min, respectively.

Tensile tests were carried out on an INSTRON 5500R test machine at 800 °C with an initial strain rate of 1.0×10^{-2} S^{-1} . Four kinds of tensile specimens were machined from both the welded blanks and base material along rolling direction, as shown in Fig. 2. After the tensile test, the specimens were quenched in cold water immediately to preserve the deformed microstructure.

The HPGF formability tests for TA15 welded tube were performed on the platform developed by Harbin Institute of Technology [11]. The laser-welded TA15 Ti-alloy tubes used in this experiment were fabricated by U-O forming method [12]. The tube is 40mm in outer diameter, 200 mm in length and 2 mm in thickness. The length of bulging zone in this test is 40mm as the same as the outer diameter of the tube. Microstructural examination was performed on a Keyence VHX-1000 microscope. The microhardness test of the weld joint was performed on a Vickers microhardness machine with load of 450N and 15 s holding time.

3. Results and discussion

Figure 3(a) is the transverse section view of a typical LBW joint in the as-welded condition, in which three distinct regions, i.e., the fusion zone(FZ), heat-affected zone (HAZ), and the base material(BM), are obvious. Figure 3(b) shows the microstructure of FZ, from which one can find that the βg grain boundaries are clearly revealed. The FZ consists of coarse columnar grains with fine acicular α' in the β matrix. The microstructure of HAZ is more complicated than that of FZ, which contains a mixture of α', primary α phases, β phases and transformed gβ phases, as shown in Fig. 3(c).

The inhomogeneity of microstructure will result in the diversity of mechanical property, so the hardness test was carried out for the joint. The typical hardness distribution is shown in Fig. 4, from

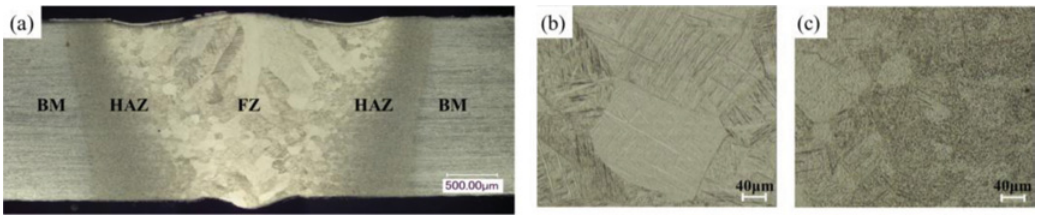

Figure 3. Microstructure of the joint (a) macro-section (b) FZ (c) HAZ.

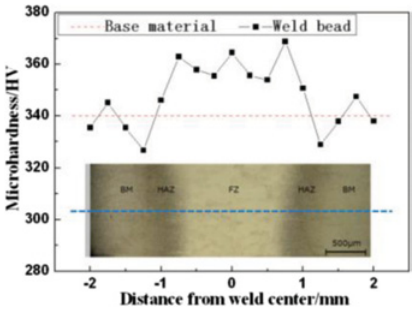

Figure 4. Hardness distribution of the as-welded joint.

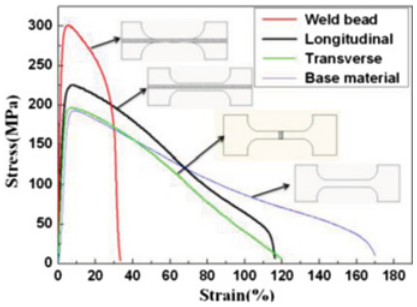

Figure 5. True stress-true strain curves.

Figure 6. Tensile specimens of (a) Weld bead (b) longitudinal specimen (c) transverse specimen (d) base material specimen.

which one can see that the FZ has the highest Vicker's hardness, due to the formation of fine acicular α' martensitic structure. Then the hardness drops rapidly in the adjacent HAZ and the BM has the lowest hardness. The FZ has Vicker's hardness ranging from 353.86 $\sim$ 368.81, the HAZ has Vicker's hardness ranging from 346.00 $\sim$ 362.91 and the BM has Vicker's hardness ranging from 326.65 $\sim$ 347.53.

The true stress-true strain curves and the specimens after deformation are shown in Fig. 5 and Fig. 6 respectively. One can see that the weld bead has the highest strength but also the lowest ductility, which is consistent with the microstructure characteristic of the coarse columnar grains with fine acicular α' in the β matrix.

The longitudinal specimen has a "sandwich" structure with the weld bead in the middle of BM. During the deformation process, the loading direction is parallel with the weld bead. The weld and base material carry the load together, so the peak stress and total elongation of the "sandwich" structure is between that of the weld bead and base material. From the true stress-true strain curves one can see that the true strain of the longitudinal specimen before failure is almost 120%, but by checking the specimen after the deformation in Fig. 8(b), one could also find that the welded material failed earlier and lots of cracks and holes formed inside the welded part due to the poor ductility.

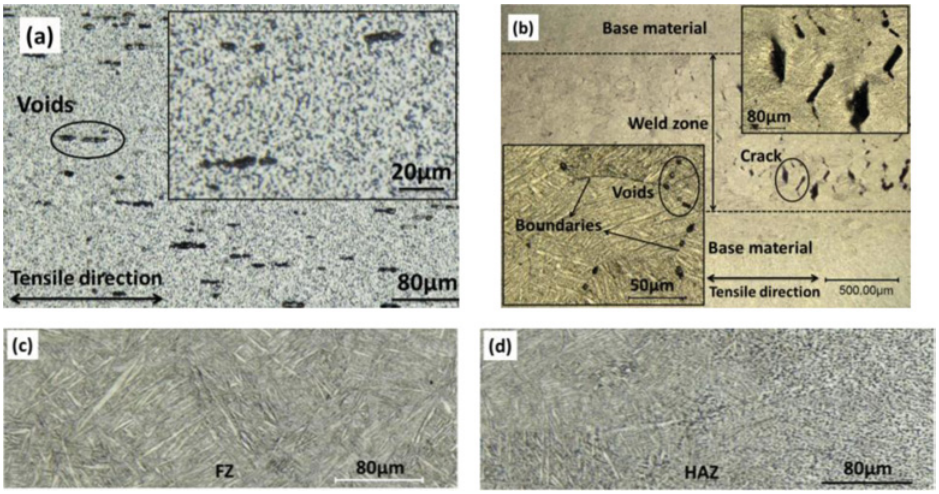

Figure 7. Microstructure after deformation (a) base material specimen (b) longitudinal specimen (c) FZ part of transverse specimen (d) HAZ part of transverse specimen.

For the transverse specimen, the loading direction is vertical with the weld bead. From the stress-strain curves one can see that compared with the base material specimen, the transverse specimen has almost the same peak stress but a much lower elongation. By checking the specimen after the deformation in Fig. 8(c), one could further find that the welded material deformed little during the tensile process, which is consistent with the microstructure and microhardness results.

The total elongation of the base material specimen is 447%, which exhibits the characteristic of superplasticity [13]. Figure 7(a) shows the microstructure of basal material specimen after failure and the picture was taken near the fracture surfaces. One can see that lots of voids formed in the triple point of grain boundaries, which was considered to be the results from grain boundary sliding (GBS) [14, 15]. The deformation mechanisms of SPF were well studied [14], and it was GBS accompanied with dynamic recrystallization (DRV) in our case [12].

Figure 7(b) shows the microstructure of longitudinal specimen after failure and the picture was taken near the fracture surfaces. One can see that in the weld zone, the fine acicular α' transformed into thicker α lamella and the aspect ratio decreased greatly which was the preliminary stage of globularization. Nevertheless, during the deformation process, the voids appeared along the β grain boundaries as the local stress excessed the limit, which leaded to the failure of the welded material. As for the transverse specimen, the microstructure of the joint after deformation is shown in Fig. 7(c) and (d), from which one could see that the lamella structure thickened obviously but no globularization happened due to the little deformation and low temperature.

From the aforesaid analysis, one could find that the microstructure has a great impact on the deformation behaviour and mechanism. In the following part, the deformation behaviour of laser-welded tubes were studied. The formability of the laser-welded tube was tested by HPGF. The loading path and corresponding bulging height curve of the apex in the weld bead are shown in Fig. 8. The demonstration is shown in Fig. 9, from which one could see clearly that the welded tube has a very good formability under 800 °C. The maximum perimeter along the hoop direction after deformation is 220 mm, so the bulging ratio of the welded tube is 77.4%.

Another interesting thing is that the tube failed at base material rather than weld bead and the crack which happened during the tensile deformation when the loading direction is parallel with the weld bead, did not occur in the HPGF. During the HHPF, the hoop strain is bigger than the axial strain, so

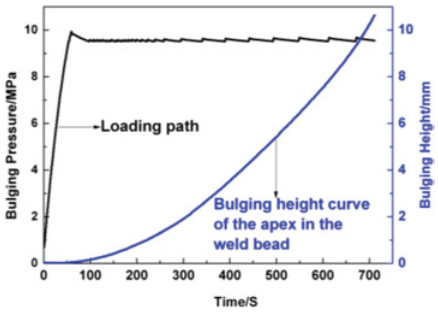

Figure 8. Loading path and bulging height curve.

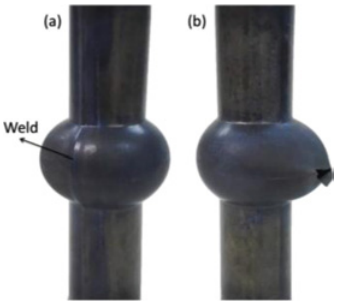

Figure 9. Formed part (a) front side (b) back side.

the weld bead endured relatively small deformation along the axial direction. After deformation, the weld bead in the bulging zone had an elongation ratio of 25% along the axial direction. Accordingly, the weld bead stayed safely during the deformation, which assured the welded tube a good formability under HPGF condition.

4. Conclusion

In this paper, deformation behaviour of laser-welded tube blank of TA15 Ti-alloy at elevated temperature was investigated by both hot tensile tests and high pressure gas forming (HPGF). The hot tensile tests were carried out on four different specimens at 800 °C with an initial strain rate of $1.0 \times 10^{-2}\,s^{-1}$ and HPGF experiment was performed at 800 °C with a constant pressure of 9.5 MPa. The following conclusions are drawn from the above work:

(1) The microstructure in the laser-welded joint is inhomogeneous. FZ consists of coarse columnar grains with fine acicular α' in the β matrix; The HAZ contains a mixture of α', primary α phases, β phases and transformed β phases.
(2) FZ has the highest Vicker's hardness, due to the formation of fine acicular α' martensitic structure. The hardness drops rapidly in the adjacent HAZ and the BM has the lowest hardness. The weld bead has a higher strength but a lower ductility than the base material.
(3) The base material with equiaxed microstructure exhibited the characteristic of superplasticity with a total elongation of 447%, and GBS accompanied with DRV was the main deformation mechanism.
(4) The weld bead has coarse columnar grains with fine acicular α' in the β matrix. When the loading direction is parallel with the weld bead, the fine acicular α' transformed into thicker lamella and the aspect ratio decreased greatly, and voids formed along the initial coarse β grain boundaries. When the loading direction is vertical with the weld bead, the welded materials deformed little and the lamella structure thickened obviously after deformation.
(5) During the HPGF experiments, the laser-welded TA15 tube has a very good formability at 800 °C, and the maximum bulging ratio is as high as 77.4%.

This work was financially supported by Program for Changjiang Scholars and Innovative Research Team in University (No. IRT1229).

References

[1] C. Leyens, M. Peters, Titanium and titanium alloys, Wiley Online Library (2003)
[2] D. Sanders, P. Edwards, G. Grant, M. Ramulu, A. Reynolds, J Mater Eng Perform, **19**, 515 (2010)
[3] D.G. Sanders, M. Ramulu, P.D. Edwards, Materialwiss Werkst, **39**, 353 (2008)
[4] S. Wang, M. Wei, L. Tsay, Mater Lett, **57**, 1815 (2003)
[5] E. Akman, A. Demir, T. Canel, T. Sınmazçelik, J Mater Process Tech, **209**, 3705 (2009)
[6] C. Kratzsch, P. Abels, S. Kaierle, R. Poprawe, W. Schulz. International Society for Optics and Photonics, 472 (2000)
[7] S. Semiatin, V. Seetharaman, I. Weiss, Mat Sci Eng A., **243**, 1 (1998)
[8] J. Shaosong, L. Baoyong, L. Yang, Z. Kaifeng, Advances in Mechanical Engineering, **2014** (2014)
[9] S. Chen, J. Huang, D. Cheng, H. Zhang, X. Zhao, Mat Sci Eng A., **541**, 110 (2012)
[10] W. Gang, W.-c. ZHANG, G.-l. ZHANG, Z.-l. XU, T Nonferr Metal Soc, **19**, s429 (2009)
[11] G. Liu, J. Wang, K. Dang, Z. Tang, Materials, **7**, 5992 (2014)
[12] B.B.K. G. Liu, W. Yang, K. H. Wang, Mater Res Innov, **19**, 6 (2015)
[13] J. Sieniawski, M. Motyka, J Achievements Mat Manufac Eng, **24**, 123 (2007)
[14] J.S. Vetrano, E.P. Simonen, S.M. Bruemmer, Acta Mater, **47**, 4125 (1999)
[15] J. Lin, Y. Liu, T. Dean, International Journal of damage mechanics, **14**, 299 (2005)